European Journal of Pharmaceutical Sciences 226 (2026) 107646

Contents lists available at ScienceDirect

European Journal of Pharmaceutical Sciences

journal homepage: www.elsevier.com/locate/ejps

Evaluation of Citicoline-loaded Lutrol 127/Carbopol/Hyaluronic acid-based gels for brain delivery by intranasal administration

Anna Patrizia de Nichilo [a,1], Francesca Uberti [b,1], Adriana Trapani [a,*], Stefano Castellani [c], Giorgia Iaconisi [d], Giorgia Franzino [e], Cinzia Di Franco [f], Lorenzo Guerra [g], Rosanna Mallamaci [g], Rosa Angela Cardone [g], Carmelo Ventra [h], Domenico Larobina [e], Loredana Capobianco [d], Simone Mulè [b], Elvira De Giglio [i]

[a] Department of Pharmacy-Drug Sciences, University of Bari "Aldo Moro", via E. Orabona, Bari, 4-70125, Italy
[b] Department for Sustainable Development and Ecological Transition, University of Piemonte Orientale (UPO), Piazza Sant'Eusebio 5, Vercelli, 13100, Italy
[c] Department of Precision and Regenerative Medicine and Ionian Area (DiMePRe-J), University of Bari "Aldo Moro", Bari, 70125, Italy
[d] Department of Biological and Environmental Science and Technology, University of Salento, Via Lecce—Monteroni, Lecce, 73100, Italy
[e] Consiglio Nazionale delle Ricerche Istituto per i Polimeri, Compositi e Biomateriali P. le Enrico Fermi, Naples, 1 80055, Italy
[f] CNR-IFN Bari, Bari Via Amendola 173, 70126 Bari, Italy
[g] Department of Biosciences, Biotechnologies and Environment, University of Bari "Aldo Moro", Bari, 70125, Italy
[h] Esseti Farmaceutici, Via Cavalli di Bronzo, 39-46, San Giorgio a Cremano, Naples, 80046, Italy
[i] Department of Chemistry, University of Bari "Aldo Moro", Bari, 70125, Italy

ARTICLE INFO

Keywords:
Citicoline gels
Rheological tests
In vitro release kinetic
Co-culture of primary nasal epithelial and SH-SY5Y neuronal cell lines
Neuroinflammation

ABSTRACT

The aim of this work was to evaluate two nasal gels specifically designed to meet three essential criteria: a suitable formulation for nasal administration, a pH compatible with the nasal mucosa, and the encapsulation capacity of the antioxidant Citicoline (CIT), which showed beneficial effects in neurological disorders such as Parkinson's disease. Hence, Carbopol 1342 (Carb) at different weights (5 mg or 25 mg), PF-127 and Hyaluronic acid (HA) provided two gelled systems, denoted as PF-127/Carb-5-HA" and "PF-127/Carb-25-HA", respectively. Gel mechanical and microstructural characterization was conducted using rheological tests and SEM observations. Moreover, *in vitro* CIT release in simulated nasal fluid showed a consistent burst effect for both gels. *Ex vivo* permeation studies using excised porcine nasal mucosa mounted on Franz cells confirmed that limited extent of CIT permeated from both formulations (7.8–9.5%). Interestingly, none of the gels was cytotoxic against the primary nasal epithelial cells (pNEC) and also when pNEC were co-cultured with the neuronal SH-SY5Y cells in order to provide an *in vitro* model of nose-brain axis (NBA). Finally, by SIRT1 quantification in the NBA model, the gels evidenced an effective neuronal inflammatory modulation, so being promising for nerve cell protection.

1. Introduction

Citicoline (5′-O-[hydroxy({hydroxy[2(trimethylammonio)ethoxy] phosphoryl}oxy)phosphoryl]cytidine, CIT) exerts beneficial effects in a variety of Central Nervous System (CNS) injuries and neurodegenerative diseases in humans. It has been applied for the improvement in the regeneration of injured nerves, for preventing the disruption of neuronal membranes and the apoptosis of neuronal cells, such as retinal ganglion and amacrine cells (Parisi et al., 2018; Roberti et al., 2014). In addition, there are several studies suggesting the antioxidant mechanism of CIT (Castellani et al., 2024a; Garcia-Lopez et al., 2023; Margari et al., 2022) which can also be beneficial in the neurodegenerative disorders, where mitochondrial dysfunction plays a crucial role and, hence, CIT can antagonize the resulting oxidative stress (Hinz et al., 2024; Salmina et al., 2021; Sathyamurthy et al., 2024).

However, the hydrophilicity of CIT and its prompt metabolism are the two main features of this active pharmaceutical ingredient (API) hindering the overcoming of the blood-brain barrier (BBB) and, as consequence, its effective formulations at CNS level should be able to bypass such obstacle. In this regard, in the last years, most interest has

* Corresponding author.
E-mail address: adriana.trapani@uniba.it (A. Trapani).
[1] These authors contributed equally to this work.

https://doi.org/10.1016/j.ejps.2026.107646
Received 6 June 2026; Received in revised form 6 August 2026; Accepted 20 August 2026
Available online 21 August 2026
0928-0987/© 2026 The Author(s). Published by Elsevier B.V. This is an open access article under the CC BY-NC-ND license (http://creativecommons.org/licenses/by-nc-nd/4.0/).

been focused on the intranasal delivery since it offers several advantages over the oral administration including the avoidance of first-pass metabolism and rapid onset of action (Crowe and Hsu, 2022; Koo et al., 2024). Moreover, one of the most interesting benefits of intranasal drug administration is the possibility to follow the nose-to-brain delivery transport pathway, enabling a variety of neuroactive agents to be conveyed directly to the brain in therapeutic amounts. It exploits the existing connections, occurring in the superior olfactory region of the nasal cavity, between the olfactory or the trigeminal nerve and the frontal region of the brain (Crowe and Hsu, 2022; Koo et al., 2024).

In the context of the nose-to-brain delivery, we have recently reported that "slightly viscous dispersions" (SVDs) can be considered possible alternative vehicles to the widely employed thermosensitive *in situ* gels, since these formulations are not devoid of drawbacks (Castellani et al., 2024b). Indeed, these last include *i*) possible toxic effects at brain level due to the higher amount of mucoadhesive polymer occurring in the preparation of thermosensitive hydrogels; *ii*) not wide availability of delivery devices able to supply sufficient dose of therapeutic agent to the superior olfactory region of the nasal cavity because all the existing ones run with liquids and powders but not with hydrogels at high viscosity as thermosensitive hydrogels (Castellani et al., 2024b).

As for CIT, it should be pointed out that this API has been already incorporated into 2-hydroxyethyl methacrylate-based hydrogels (Teixeira et al., 2024) or blends alginate and sterculia gum (Singh et al., 2020) and it was demonstrated that such dosage forms constitute efficient drug release platforms for the treatment of neurodegenerative diabetic ocular diseases. In addition, recently, several nanocarriers have been proposed for the brain delivery of CIT including solid lipid nanoparticles (Castellani et al., 2024a), ultra-flexible transbilosomes (TBLs) which are nanovesicular systems mostly made of non ionic surfactants and bile salts (AbouElhassan et al., 2022) and Niosomal in situ gel (Bekhet et al., 2022). However, to the best of our knowledge, CIT-loaded polymer-based hydrogels as a novel strategy for CIT brain delivery application to date have not been described.

Going ahead in this research area, herein we wished to evaluate the potential of two gels to be administered by nasal route and possessing a pH value compatible with the nasal mucosa as alternative vehicles to the thermosensitive in situ gels in order to promote safe and efficient nose-to-brain delivery. For this purpose, we considered the combination of the polymer Carbopol with PF-127 (also known as Lutrol 127 or Poloxamer 407) which, by using appropriate mass ratios and in the presence of hyaluronic acid (HA), provides hydrogels different from the previously studied SVDs (Castellani et al., 2024b). The addition of HA was justified by some reasons as *i)* it is well known that drawbacks associated to polymeric platforms made up of Carbopol and Poloxamer 407 for drug delivery applications, such as poor mechanical proper maintaining be bypass educing low molecular weight HA (Mayol et al., 2008); *ii)* according to recent literature suggestions, addition of HA may increase the viscoelastic features of the final gel formulations (Khan et al., 2026) and finally *iii)* HA may contribute to maintain the pH value within (or very close) the range recognized as safe (pH 4.5-6.5) (Castellani et al., 2024b) to avoid the nasal mucosa irritation. Hence, the aim of the present work was to formulate and evaluate the *in vitro* performances of CIT-loaded gels for the intranasal administration of the antioxidant agent in order to enhance the absorption of this beneficial agent in the neurodegenerative disorders following the "nose--to-brain-delivery" transport pathway. For this purpose, after the details of the preparation of the gels studied, we report herein the physicochemical characterization of these CIT-loaded carriers including rheological evaluation, SEM observations, *in vitro* release tests in simulated nasal fluid (SNF), *ex vivo* permeation studies through excised nasal porcine mucosa and then they were evaluated in human cell model lines.

Concerning the selection of such cell model lines, we aimed at mimicking the neurodegenerative disorder of Parkinson disease (PD), where CIT can act for adjuvant therapy as reported elsewhere (Hamdy et al., 2025; Que and Jamora, 2021; van Brummelen and van Brummelen, 2025). It is well known that processing occurring at the nasal district and neurodegeneration typical of PD are closely related (Dorsey et al., 2024; Lazarini et al., 2022). Moreover, toxicants inhaled through the nose were seen to determine pathological changes in alpha-synuclein in the olfactory system that subsequently spread and give rise to a brain-first subtype of Lewy body disease, resembling PD (Dorsey et al., 2024). This evidence reinforces the hypothesis that a so called "nose-brain axis" (NBA) transport is operating in PD patients (Mou et al., 2024) and, being bidirectional, it requires appropriate excipients in the pharmaceutical dosage forms that should enhance such bidirectional crosstalk. After the physicochemical characterization of the gels, the co-culture of primary Nasal Epithelial Cells (pNEC) and SH-SY5Y neuronal lines allowed us to provide *in vitro* a NBA platform suitable for testing free CIT and its semisolid gels here in described. The results arising from such investigations are described and discussed in this work.

2. Materials and methods

2.1. Materials

Citicoline sodium salt (CIT) was kindly provided as a gift from Esseti Farmaceutici s.r.l. (Pomezia, Italy). Lutrol 127 (poly(ethylene oxide)-poly(propylene oxide) copolymer PF-127, Poloxamer 407) was supplied by BASF (Ludwigshafen, Germany). Carbopol 1342 (Carb, Acrylates/C10-30 Alkyl Acrylate Crosspolymer, viscosity 4,000–11,000 mPa·sec for 0.2% aqueous solution) was provided by IMCD (Milan, Italy). HA was prepared through microbial fermentation by using E. coli as bacterial host following a procedure whose protection by Italian patent is underway (Italian patent N.102025000010455). Sodium hydroxide pellets, acetic acid for rheological tests, salts for buffer preparation were bought from Sigma-Aldrich (Milan, Italy).

2.2. Preparation of PF-127/Carb/HA-based gels

The gels arising from the combination of PF-127/Carb were prepared according to the procedure previously reported with slight modifications (Mura et al., 2018). To 1 mL of distilled water, PF-127 (110 mg) was added and then the mixture was left at 4°C in the fridge for 1 h. Afterwards Carb (5 mg or 25 mg), CIT (10 mg) and HA (1 mg) were added to obtain the gel at room temperature. Herein, "PF-127/Carb-5-HA CIT" refers to the composition of 110 mg PF-127, 5 mg Carb, 10 mg CIT and 1 mg HA, whereas "PF-127/Carb-25-HA CIT" refers to the composition of 110 mg PF-127, 25 mg Carb, 10 mg CIT and 1 mg HA. Control gels were prepared as above but without CIT addition, and such CIT-unloaded gels were referred to as "PF-127/Carb-5-HA" and "PF-127/Carb-25-HA", respectively. Lyophilization of the prepared gels was performed for 72 h using a Lio Pascal 5P (Milan, Italy), providing powders employed for the following studies.

2.3. Quantitative determination of CIT

CIT quantitative determination was carried out by spectrophotometric analysis using a calibration curve obtained dissolving CIT in double distilled water (concentration range 100-1μg/mL, $R^2 > 0.999$). CIT measurements were performed at the wavelength of 280 nm by using a Perkin-Elmer Lambda Bio 20 UV-150 Vis spectrophotometer (Perkin-Elmer, Milan, Italy).

2.4. Physicochemical characterization of the gels examined

2.4.1. pH measurements

pH values of the unloaded gels (*i.e.*, PF-127/Carb-5-HA and PF-127/Carb-25-HA) and the corresponding CIT loaded ones (*i.e.*, PF-127/Carb-5-HA CIT and PF-127/Carb-25-HA CIT) were measured at 25°C by a FIVEEASY pH meter apparatus (Levanchimica, Bari, Italy). After

bringing the electrode of the pH meter near the surface of gels and allowing it to equilibrate for 1 min (Srividya et al., 2001) the pH measurement was performed. For each gel, pH measurements were carried out in triplicate and the results are expressed as means ± SD.

2.4.2. Osmolarity assessment

A VAPRO® vapor pressure osmometer 5600 (Wescor, Inc., Logan, UT, USA), with fresh 290 mmol/kg, 1000 mmol/kg and 100 mmol/kg standard solutions, following the manufacturer's instructions, was used to measure the osmolarity of pure CIT and the gels examined. A single Whatman filter paper disc (Wescor, ss-033) was placed in the central depression of the holder using metal forceps, and 10 µL of each sample were expelled onto the disc. Saturated discs were rapidly transferred to the vapor pressure osmometer sample holder, and osmolarity was determined. As mentioned below, only for PF-127/Carb-5-HA CIT the osmolarity measurement was possible, and it was performed in triplicate. The corresponding result was expressed as mean ± SD.

2.4.3. Scanning electron microscopy analysis

Scanning Electron Microscopy (SEM) analysis of CIT-loaded and unloaded gels was carried out as follows. Specimens were mounted onto double-sided carbon adhesive stubs and observed without prior metallic coating. Five non-overlapping areas per sample were systematically acquired and analyzed using a field emission scanning electron microscope (Zeiss, mod. Sigma), in-Lens detector at 1 kV, with 30 µm aperture and working distance of 4 mm.

2.5. Rheological tests on the gels studied

Rheological experiments were conducted on both gels and pre-gelled formulation by using a stress-controlled HAAKE MARS III rheometer (Alfatest, Roma, Italy). For the gelled formulations a 35 mm plate–plate geometry was used. Measurements were performed according to the following protocol: each sample was loaded at room temperature and allowed to equilibrate for 300 s to reach the desired temperature (*i.e.,* namely 37°C for neutralized gels, pH = 6). Subsequently, a pre-shear test ($\dot{\gamma} = 100\ s^{-1}$, t = 120 s) was applied, followed by a time sweep test lasting 900 s. After completion of the time sweep, frequency sweep tests were carried out at constant stress. Preliminary stress sweep tests at 37°C confirmed that all frequency sweep measurements were conducted within the linear viscoelastic region. In all experiments, a solvent trap was used to minimize solvent consumption evaporation. Measurements were performed on *i)* PF-127/Carb-5; *ii)* PF-127/Carb-5-HA; *iii)* PF-127/Carb-5-HA CIT after gelation at 37°C and pH = 6 (*i.e.*, neutralized after preparation). We also performed rheological tests on the pre-gelled formulation, precisely containing 1% w/w of Carb. Specifically, flow-curve tests were conducted using a 2° cone-and-plate geometry, applying stepwise increases in shear rate from 0.01 to 1000 s^{-1} and performing all measurements at 20°C and at the formulation's spontaneous pH.

2.6. In vitro release tests in Simulated Nasal Fluid

The *in vitro* CIT release kinetics from the gels examined were evaluated according to our previously published protocol with slight modifications (Cassano et al., 2020). Briefly, freeze-dried gels containing 600–1000 µg of CIT were suspended in 1.5 mL of double distilled water in a dialysis bag soaked in 30 mL of SNF thermostated at 37 ± 0.1°C in an agitated (40 rpm/min) water bath (Julabo, Milan, Italy). At appropriate time intervals, withdrawals of 1.5 mL were carried out and centrifuged at 16,000g, 45 min (Eppendorf 5415D, Germany) and 1.5 mL of freshly prepared SNF was adopted for replacement. The supernatant was subjected to the spectrophotometric content determination for CIT according to our previously reported protocols (Castellani et al., 2024a). The experiment for each type of gel examined was performed in triplicate and results are expressed as means ± standard deviation.

2.7. Ex vivo CIT permeation studies through excised nasal porcine mucosa

The *ex vivo* CIT permeation studies through excised nasal porcine mucosa were carried out following our previously reported protocol (Trapani et al., 2023). Briefly, such studies were performed employing a vertical Franz cell (PermeGear Inc., SES GmbH, Bechenheim) and nasal porcine mucosa obtained from pig snouts achieved from a local slaughterhouse. Before their use, a portion of the nasal mucosa was immediately stored in 10% buffered formalin and the histological examination was performed for each animal at least 72 h after fixation to rule out pathologies and mucosal damage. After treatment of tissue with paraffin, hematoxylin and eosin or periodic acid for staining, 5-µm sections were examined with a Leica DMLS D 4000 microscope equipped with digital camera (Leica DMC5400, Milan, Italy). Sections were rated by working with magnification of 200 (*i.e.,* objective 20 and eyepiece lens 10; 0.7386 mm^2 per field), subsequent to 400 field magnification (*i.e.,* objective 40 and eyepiece lens 10; 0.1885 mm^2 per field). In such experiments, the anterior surface of the mucosa was faced towards the donor compartment (effective diffusion area = 0.6 cm^2), and freeze-dried PF-127/Carb-5-HA CIT (or PF-127/Carb-25-HA CIT, or CIT powder taken as control) were resuspended in 500 µL of SNF, pH 5–6, and placed in the donor compartment. The Franz cell apparatus was maintained at 37.00 ± 0.03°C with a CD-B5 heating circulator bath (Julabo GmbH, Seelbach, Germany) for 24 h, and the acceptor compartment was filled with 5 mL of SNF in the presence of an ATE magnetic stirrer (VELP Scientifica Srl, Usmate, Italy) that allowed continuous stirring. The system was allowed to equilibrate at 37°C for 15 min, and isothermal conditions were maintained through a water jacket system. At scheduled time points (0, 1, 2, 4, 8 and 24 h), aliquots of 0.5 mL were withdrawn from the receiving chamber and refilled with 0.5 mL of fresh SNF. Each withdrawal was subjected to centrifugation (Eppendorf 5415D, Hamburg, Germany) at 13,200 g for 45 min, for discarding particles eventually diffusing as such. After centrifugation, the resulting supernatant was analyzed according to the spectrophotometric assay for CIT above described in Section 2.3. For each formulation, the permeation study was repeated in sextuplicate. The apparent permeability coefficient (P_{app}) was determined according to Equation (1):

$$P_{app} = dQ / dtAC_0 \quad (1)$$

Where dQ/dt is the cumulative amount of CIT permeated *vs* time per unit of area, in turn obtained by the slope of the linear tract of the first segment of the curve, A is the effective surface area, and $C_0$is the initial CIT concentration in the donor compartment. When the experiment was concluded, the nasal porcine mucosa was incubated with 1 mL of water overnight at 25°C to extract the retained CIT, which was then quantified *via* spectrophotometric analysis. CIT amounts recovered from the mucosa added to the CIT amounts of the acceptor and donor compartments allowed the calculation of the mass balance.

2.8. In vitro cellular studies

pNECs purchased from PromoCell (Heidelberg, Germany) were adopted to evaluate cytotoxic effects at the human airway epithelium level in which both ACE2 and TMPRSS2 receptors are expressed (Barron et al., 2021). Cells were grown using commercially available supplemental air way epithelial cell culture medium (Airway Epithelial Cell Growth Medium Ready-to-use, PromoCell, Heidelberg, Germany) at 37°C, 5% CO_2. The culture medium was replaced with fresh medium every two days until step 2 (Nantachit et al., 2016). Upon reaching 70-80% confluence, 5×10^5cells/cm^2 were seeded on a 12 mm Transwell® system with a transparent 0.4 µm polyester insert (Costar® Corning, Cambridge, MA, USA) and placed in complete medium for 72 hours to obtain a completely confluent cell layer. The apical surface was exposed to the air-liquid interface (ALI technique) for 14 days (Martens et al., 2019) to mimic the physiological conditions of the nasal

epithelium. The neuroblastoma cell line SH-SY5Y (ATCC, Manassas, VA, USA) was maintained in a 1:1 mixture of advanced DMEM F12 and advanced DMEM (GIBCO®, Thermo Fisher Scientific, Waltham, MA, USA), supplemented with 10% FBS. Cultures were incubated at 37°C in a humidified atmosphere containing 5% CO_2 (Wu et al., 2018). Experiments were conducted using SH-SY5Y cells at passages from 3 to 20 and they were grown under co-culture conditions with pNECs on the Transwell® system in order to recreate an NBA *in vitro* model (Section 2.9.4). Before each stimulation all seeded cell cultures were placed in DMEM medium free of phenol red and 0% FBS to synchronize them to the same phase of the cells *in vitro*.

The *in vitro* study was divided into two complementary phases: *in vitro* safety and biological effects on a human nasal epithelial monolayer (pNECs), and then neuronal effects resulting from nose-brain passage, using a co-culture model described in Section 2.9.4. In the first step, pNECs were seeded on Transwell® inserts and cultured in complete medium for 72 h, until a confluent monolayer was reached. Subsequently, the apical compartment was treated with gel with and without CIT compared to CIT alone, for different exposure times based on the analytical method carried out. In detail, analyses were conducted on cell viability via 3-(4,5-dimethylthiazol-2-yl)-2,5-diphenyltetrazolium bromide (MTT) assay and on oxidative stress (ROS production) after 24 h of treatment; on the integrity of the monolayer via multi-time transepithelial electrical resistance (TEER) measurements (1 h, 6 h, 12 h, 24 h); on absorption kinetics via fluorescein sodium salt (at the same TEER intervals); and on activation of the inflammatory response (TNF-α and IL-1β dosing via ELISA kit) after 24 h of treatment.

The apical metabolite produced by treating pNECs moved to the basolateral compartment of the Transwell® system, where SH-SY5Y neuronal cells were cultured, in order to test the hypothesis of translation of effects from the nasal cavity to the brain. After that, the neuronal cells were subjected to treatment for 24 h. Neuronal viability (*via* MTT assay), oxidative stress through measurement of ROS production and SOD1 levels via ELISA kit, inflammatory activation (TNF-α and IL-1β via ELISA kit), and Sirtuin 1 (SIRT1) levels as a marker of neuronal well-being were also assessed through ELISA kit. The collected data were statistically analysed to verify any significant differences between treatments and controls.

2.9. Cell viability

Applying the MTT *in vitro* Toxicology Assay Kit (Merck Life Science, Rome, Italy), cell viability was verified on every experimental protocol phase following each stimulation in agreement with a standard procedure reported in the literature (Ferrari et al., 2024). All solubilised samples, both treated and untreated, were measured at the wavelength of 570 nm with correction at the wavelength of 690 nm using a spectrometer (Infinite 200 Pro MPlex, Tecan, Männedorf, Switzerland). The findings were shown as the average ± standard deviation (%) of viable cells relative to the control (untreated samples) of five independent experiments performed in triplicate.

2.9.1. Reactive Oxygen Species (ROS) production

The rate of superoxide anion release in the nasal epithelium and in the SH-SY5Y cells was measured using the method based on cytochrome C reduction (Galla et al., 2022). For 30 minutes, both treated and untreated cells were incubated with 100 μL of cytochrome C and 100 μL of superoxide dismutase (Merck Life Science, Rome, Italy). The absorbance in culture supernatants was measured at the wavelength of 550 nm using a spectrometer (Infinite 200 Pro MPlex, Tecan, Männedorf, Switzerland). ROS production is defined as the mean ± SD (%) of nanomoles of reduced cytochrome C per microgram of protein in comparison to the control (0 line) of five separate experiments carried out in triplicate.

2.9.2. Transepithelial Electrical Resistance (TEER) measurement for barrier integrity

Prior to starting the stimulations with test samples, complete differentiation of nasal epithelia cultured on permeable inserts was confirmed by TEER measurement using the EVOM3 volt-ohmmeter (World Precision Instruments, Sarasota, FL, USA). Only inserts that reached a TEER value greater than 300 Ω•cm^2 were considered suitable for the experiments (Martens et al., 2019). During stimulation with samples, epithelial barrier integrity was monitored by successive TEER measurements at the following time points: 1 hour, 6 hours, 12 hours and 24 hours. Before each measurement, the inserts were kept at room temperature for 15 minutes to stabilize the electrical values. TEER was measured by placing the volt-ohmmetric electrodes on the insert, ensuring optimal contact with the basal and apical medium. The obtained values were normalized by subtracting the background resistance measured on cell-free inserts and multiplying by the insert area, expressing the results in Ω•cm^2.

2.9.3. In vitro permeability studies

Fluoresce in sodium salt (Santa-Cruz, CA, USA) at the concentration of 0.04% was used to detect the permeability rate at each time point in nasal epithelium after the treatment with each sample (Galla et al., 2021; Moratin et al., 2025). pNECs were incubated for 40 minutes at the previously mentioned concentration to quantify the amount of fluorescein transported at 37°C. An Infinite 200 Pro MPlex equipment (Tecan Männedorf, Switzerland) was used to detect fluorescence at excitation and emission wavelengths of 490 and 514 nm, respectively. The following equation was used to calculate the permeation rate (Equation (2):

$$J = Jmax[C]/(Kt + [C]) \quad (2)$$

Where:

- Jmax: the maximum permeation rate;
- [C]: the initial concentration of fluorescein;
- Kt: Michaelis–Menten constant determined according to King's work (King et al., 2021).

Results are expressed as mean ± SD (%). Negative controls without cells were tested to exclude the influence of the Transwell® membrane.

2.9.4. Co-culture model of the NBA in vitro

The pNECs generated by ALI culture as described in Section 2.8, were used to obtain a co-culture model adding to the basolateral side neuronal cells, in order to evaluate the interactions nose to brain. In particular, from 3×10^3 to 1×10^5 SH-SY5Y cells/cm^2 within 14 passages (Pichla et al., 2020) were seeded in a 24 well and after 48h the cells were differentiated using Neurobasal medium (containing B27 supplement and GlutaMAX, Thermo Fisher Scientific, Waltham, Massachusetts, USA) supplemented with 10 μM all-trans retinoic acid (Merck Life Science, Milan, Italy) for 7 days to obtain neuron-like cells monitoring the neurite outgrowth (Kovalevich and Langford, 2013). When SH-SY5Y cells produced a neuronal phenotype and pNECs had re-created a pseudostratified mucociliary epithelium, both cell types were assembled, and the co-culture was stimulated.

2.9.5. SOD-1 production assay

Using SH-SY5Y cell lysate, the SOD level was determined in agreement with the manufacturer's instructions (Cayman's Superoxide Dismutase Assay Kit; Tallinn, Estonia) (Uberti et al., 2023). By comparing data to a standard curve (0.05–0.005 U/mL), the amount of SOD contained in cell lysates was determined. A spectrometer (Infinite 200 Pro MPlex, Tecan, Männedorf, Switzerland) was used to measure the absorbance of each sample in the wavelength range 440–460 nm. The data were reported as means (%) in relation to the control of five different experiments performed in triplicates.

2.9.6. TNF-α production ELISA kit

TNF-α measurement in the nasal epithelium supernatants and SH-SY5Y cells was performed using the TNF-α ELISA kit (Merck Life Science, Rome, Italy) according to the manufacturer's guidelines (Molinari et al., 2021). The samples absorbance was measured at the wavelength of 450 nm with a plate reader (Infinite 200 ProMPlex, Tecan, Männedorf, Switzerland). The outcomes were obtained utilising a calibration curve (range: 24.6–6000 pg/mL) and are presented as mean values ± SD (%) to the control (0 line) from five independent experiments conducted in triplicate.

2.9.7. IL-1β production ELISA kit

IL-1β levels in the nasal epithelium and SH-SY5Y cells lysates were measured according to the manufacturer's guidelines with an IL-1β ELISA Kit (R&D Systems, Minneapolis, MN, USA). The absorbance was assessed using a microplate reader at 450 nm, with a correction at 570 nm. The quantification of IL-1β involved comparing the measurements with the obtained standard curve (3.9–250 pg/mL, (Xu et al., 2015). Results are expressed as mean values ± SD (%) to the control (0 line) from five independent experiments conducted in triplicate.

2.9.8. Sirt-1 ELISA kit

The Sirtuin 1 protein (Sirt-1) was quantified with the Human SIRT1 ELISA kit (ThermoScientific™, Waltham, MA, USA) on the SH-SY5Y lysate. An Infinite 200 Pro-MPlex apparatus (Tecan, Männedorf, Switzerland) was used to detect the absorbance at 450 nm following the addition of 50 µL of stop solution to each well. The results are shown as a percentage (%) of the control (line 0, untreated cells) from five separate experiments, each carried out in triplicate. The concentration is reported as ng/mL and the reference standard curve ranged between 1.2 and 300 ng/mL (Galla et al., 2025).

2.10. Statistical analysis

Physicochemical data are presented as mean ± SD. Multiple comparisons were based on one-way analysis of variance (ANOVA), with Bonferroni's post hoc test, and differences were considered significant when $p < 0.05$. Statistical evaluation was performed with Prism v. 5.0 (GraphPad Software Inc., La Jolla, CA, US). Biological data are presented as mean ± standard deviation and are derived from at least five biological replicates, each carried out in triplicate. Using GraphPad Prism 10.2.3 software (GraphPad Software, La Jolla, CA, USA), statistical analysis was carried out using a one-way ANOVA followed by either the Mann–Whitney U test or Bonferroni's post hoc test. Data were normalized as percentages in relation to control values, and differences were deemed statistically significant at $p < 0.05$.

3. Results

3.1. Characterization of the gels studied

The CIT-loaded gelled formulations were prepared as above described and characterized in order to assess if they can be suitable for a nose-to-brain delivery application. First of all, the gels studied were evaluated as for their pH values taking into account the mentioned importance of this parameter to avoid nasal mucosa irritation. In particular, it was found that for PF-127/Carb-5-HA and for PF-127/Carb-25-HA the pH values were 3.8 ± 0.3 and 4.1 ± 0.2, respectively. On the other hand, the pH values of PF-127/Carb-5-HA CIT and PF-127/Carb-25-HA CIT were found equal to 4.0 ± 0.1 and 4.5 ± 0.2, respectively. Regarding osmolarity data, PF-127/Carb-5-HA CIT showed a value of 54 ± 1 mOsm/kg, an osmolarity value very similar to that found for an aqueous solution of pure CIT (10 mg/mL), suggesting that in both cases the osmotic effect was almost negligible. On the other hand, likewise due to the high viscosity of PF-127/Carb-25-HA CIT gel, no osmolarity measurement was possible in the experimental conditions used.

3.2. SEM observations

SEM micrographs (Fig. 1A-D) highlighted clear morphological differences among the investigated gel formulations. At lower Carb concentration *(i.e.*, PF-127/Carb-5-HA, Fig. 1A), the structure appeared lamellar and discontinuous, characterized by irregularly folded layers and the presence of fissures and interlaminar gaps rather than a well-defined porous network. The surface is heterogeneous, with evident structural fragmentation. Upon increasing the Carb content (PF-127/Carb-25-HA, Fig. 1B), the morphology transitions toward a more cohesive and compact matrix were evidenced. Although voids were still detectable, they appeared less extensive and more embedded within a continuous polymeric framework, suggesting improved structural organization and higher matrix packing. Indeed, the addition of CIT further modulated the microstructure. PF-127/Carb-5-HA CIT (Fig. 1C) exhibited a more entangled and interconnected architecture compared to its non-CIT counterpart, with reduced lamellar separation and a more uniform distribution of structural domains. In contrast, PF-127/Carb-25-HA CIT (Fig. 1D) displayed a highly compact and continuous surface, largely devoid of visible fissures or macroporous features, indicative of enhanced structural integration within the polymeric network.

3.3. Rheological evaluation

Before evaluating the rheological features of the gels studied, we considered of interest to investigate the rheological behavior of the PF127/Carb-1-HA CIT formulation (*i.e.,* exceptionally adopting Carbopol at 1% w/w for experimental needings), since useful information even for the other gels herein examined can be deduced. Thus, the steady-shear behavior of this last formulation prepared with 1% w/w of Carb was evaluated at temperature of 20°C and at the formulation's spontaneous pH value of 3.9. As displayed in Fig. 2A the resulting shear-viscosity curve shows a pronounced decrease in viscosity with increasing shear rate, typical of a shear-thinning fluid, confirming that the material behaves as a structured viscous liquid.

Then, due to the difficult solubilization of Carb alone in aqueous medium at concentrations higher than 1% w/w, the rheological evaluation focused on the following systems: PF-127/Carb-5, PF-127/Carb-5-HA and PF-127/Carb-5-HA CIT. Upon neutralization up to pH 6 (the

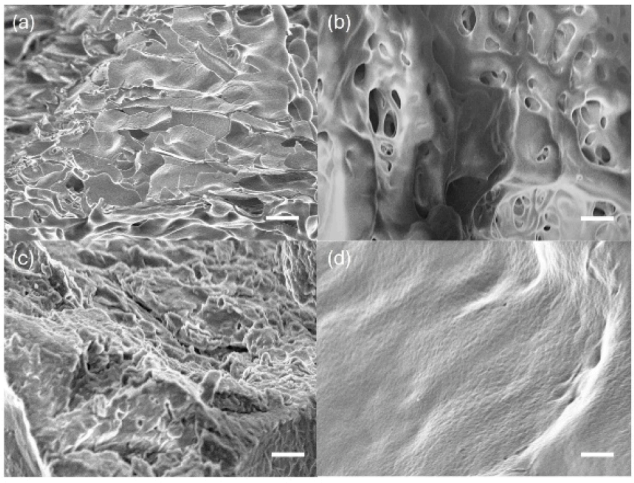


Fig. 1. SEM micrographs of (a) PF-127/Carb-5-HA, (b) PF-127/Carb-25-HA, (c) PF-127/Carb-5-HA CIT, and (d) PF-127/Carb-25-HA CIT. Representative images highlight the morphological differences among the formulations in terms of structural organization and surface compactness. The white scale bar corresponds to 10 µm. Images were acquired at EHT 1 kV using an in-lens detector, with a working distance (WD) of 4 mm.

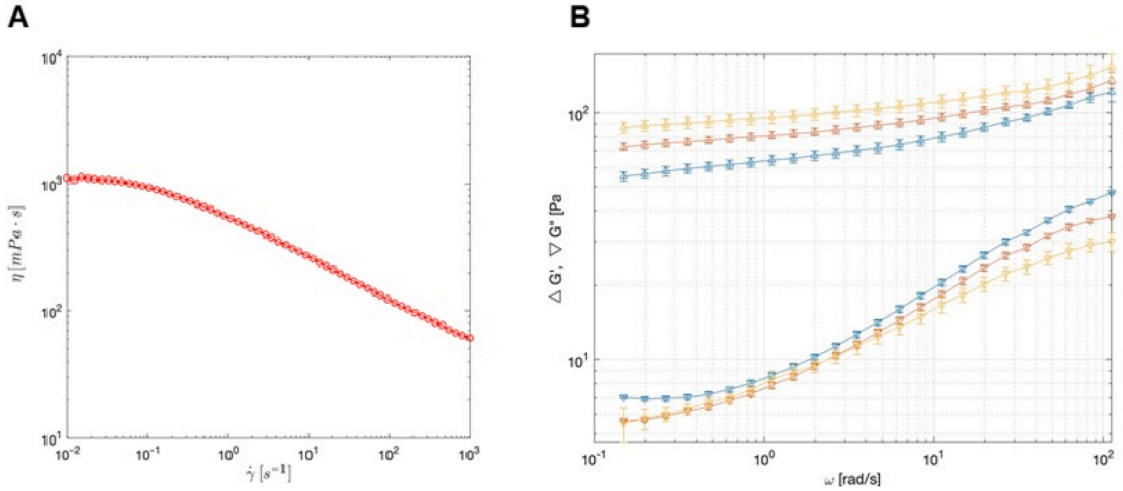


Fig. 2. Panel A: Flow curve of PF127/Carb-1-HA CIT at T=20°C and pH=3.9. Panel B: Frequency-dependent storage (G′) and loss (G″) moduli for PF-127/Carb-5 (yellow), PF-127/Carb-5-HA (red), and PF-127/Carb-5-HA CIT (blue) at 37°C. G″ remains approximately constant across all formulations, while G′ decreases progressively from PF-127/Carb-5 (highest) to PF-127/Carb-5-HA (intermediate) and PF-127/Carb-5-HA CIT (lowest), indicating a weakening of the elastic network upon addition of HA and CIT.

same of the nasal cavity) and heating to 37°C, all samples underwent a marked sol–gel transition, forming relatively stronger physical gels. As shown in Fig. 2B, the storage modulus G′ decreased progressively across the three formulations: PF-127/Carb-5 exhibited the highest G′, PF-127/Carb-5-HA showed an intermediate value, and PF-127/Carb-5-HA CIT displayed the lowest. In contrast, the loss modulus G″ remains nearly constant throughout, indicating that viscous dissipation is largely unaffected by the addition of HA and CIT. From a material point of view, the sequential addition of HA and CIT seems to weaken the elastic network formed by PF-127 and Carb, likely by disrupting microgel packing or modifying interfacial interactions, without any significant altering frictional losses.

3.4. *In vitro release studies*

An *in vitro* release study of CIT from PF-127/Carb-5-HA CIT and PF-127/Carb-25-HA CIT gels was conducted to investigate the effect of the different formulations on the release of antioxidant agent during an incubation time of 48 h at 37°C in SNF (Fig. 3A). In particular, a burst effect of CIT release was provided by both gels and appreciable percentages of the delivered antioxidant agent till the end of the release test were detected (up to 95% at 48 h from PF-127/Carb-5-HA CIT and up to 100% at 48 h from PF-127/Carb-25-HA CIT, Fig. 3A). Overall, the most interesting data from *in vitro* release studies from gel samples were that both of them released CIT in essentially quantitative amounts after 48 h of release time even though the CIT release from PF-127/Carb-25-HA CIT gel resulted slightly faster than PF-127/Carb-5-HA CIT.

3.5. *Mucosal permeation experiments*

Gel effects on CIT permeability through excised porcine nasal mucosa were investigated with Franz diffusion cells (Fig. 3B and Table 1). Interestingly, for PF-127/Carb-5-HA CIT and PF-127/Carb-25-HA CIT

Table 1
P_{app} of CIT after exposure of the porcine mucosa to different gels through Franz cells. $^{**}p < 0.001$.

Formulation	P_{app} (cm/sec)	CIT permeated (%)	CIT extracted from the nasal porcine mucosa (%)	CIT retained in the apical side (%)
Pure CIT	$12.3\times10^{-3}\pm 1\times10^{-4}$	8.9±2.2	1.9±0.1	89.1±3.8
PF-127/Carb-5-HA CIT	$9.9\times10^{-3}\pm 3\times10^{-3}$	9.5±0.6	7.0±0.8**	83.5±4.6
PF-127/Carb-25-HA CIT	$7.2\times10^{-3}\pm1.5\times10^{-3}$	7.8±1.8	1.7±0.5	90.4±0.7

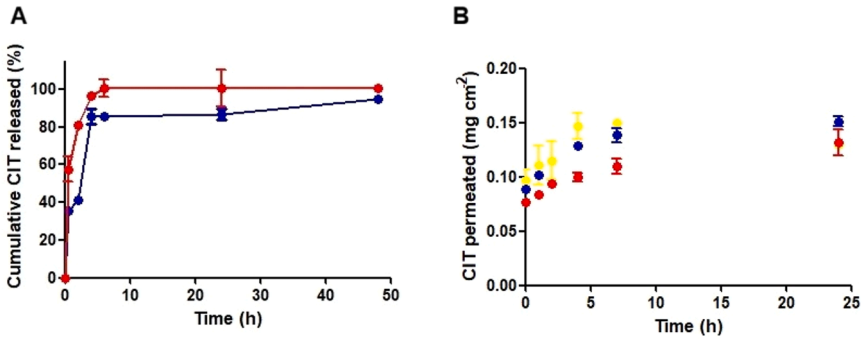


Fig. 3. Panel A: Cumulative CIT release profiles in SNF from PF-127/Carb-5-HA CIT (blue) and from PF-127/Carb-25-HA CIT (red). Data are mean values ± SD (n = 3). Panel B: *Ex vivo* permeation profiles through excised nasal porcine mucosa of free CIT (yellow filled circles), from PF-127/Carb-5-HA CIT (blue filled circles) and from PF-127/Carb-25-HA CIT (red filled circles). Data represents mean values ± SD (n = 3).

the values of apparent permeability coefficient (*P*app) were equal to 9.9 × 10^{-3} ± 3 × 10^{-3} and 7.2 × 10^{-3} ± 1.5 × 10^{-3} cm/sec, respectively, vs 12.3 × 10^{-3} ± 1 × 10^{-4} cm/sec referred to pure CIT (Table 1), but no statistical difference was found between *P*app of free CIT and each one of the tested gels. Similarly, from Table 1, among all the tested samples the permeated CIT percentage across the porcine nasal mucosa was comparable, being in the range 7.8–9.5% of the initial CIT content, whereas the percentage of CIT extracted from the mucosa ranged between 1.7–7.0% in good agreement with no color change in such tissue extracts. In addition, no visual change in the SNF receiving medium was detected through the experiments for all the tested gels and free CIT.

Surprisingly, as shown in Table 1, for gels and CIT the percentage of the antioxidant retained in the apical side was found in the range 83.5% and 90.4% in comparison to the initial CIT content.

3.6. *In vitro assessment of the biological effects of gels on the nasal epithelium*

As shown in Fig. 4A, all the formulations analysed showed a good tolerability profile on the nasal epithelium reconstituted *in vitro*, without inducing any cytotoxic effect after 24 hours of exposure. In particular, control gels and CIT-gels maintained levels of cell viability comparable or higher than the untreated control (line 0%), indicating good biocompatibility of the vehicle itself. Precisely, PF-127/Carb-25-HA showed a statistically significant increase in cell viability compared to the control (Fig. 4A, $p < 0.05$), whereas both PF-127/Carb-5-HA CIT and PF-127/Carb-25-HA CIT did not alter the observed safety profile compared to the control.

Moreover, the data obtained from the evaluation of oxidative stress is consistent with those of cell viability (Fig. 4B). All treated samples showed a significant reduction in ROS levels compared to the control, indicating good antioxidant activity. Both PF-127/Carb-5-HA and PF-127/Carb-5-HA did not cause any increase in ROS levels compared to control (Fig. 4B). Furthermore, PF-127/Carb-5-HA CIT and PF-127/Carb-25-HA CIT did not cause an adverse effect in terms of increased ROS levels and, particularly, PF-127/Carb-25-HA CIT stood out for its effectiveness in reducing oxidative stress compared to PF-127/Carb-5-HA ($p < 0.05$) (Fig. 4B).

To gain insight into the behaviour of the gels in the nasal compartment, TEER measurements proved to be a fundamental tool for monitoring the functional integrity of the nasal epithelial monolayer exposed to the different treatments over time (Fig. 5A).

As shown in Fig. 5A, all samples tested maintained TEER values consistently above the physiological integrity threshold (cut-off: 300 Ω·cm^2) for the entire duration of the observation. These values were significantly higher than those of the untreated control ($p < 0.05$), indicating not only the absence of cytotoxicity effects, but also a potential contribution to the maintenance of the nasal epithelial barrier. Consistently with the data obtained from cell viability and oxidative stress assays, the formulation PF-127/Carb-25-HA CIT provided TEER values slightly higher than PF-127/Carb-5-HA CIT in terms of preservation of epithelial integrity, but its TEER values were lower than those obtained with CIT alone and higher than those of the control gels ($p < 0.05$). Indeed, a similar trend was observed in Fig. 5B for PF-127/Carb-5-HA, whereas the use of PF-127/Carb-5-HA CIT resulted in a significant TEER increase compared to the gel without CIT and to the control ($p < 0.05$).

Further data were obtained through the studies on the absorption kinetics of CIT alone and in the gels through the nasal epithelium using fluorescein as probe (Fig. 5C and 5D). The data obtained highlighted a role of greater permeability enhancement due to PF-127/Carb-25-HA CIT in the frame time of 1h-4h range with statistically significant data only in the 1h-2h range (*i.e.,* 38% increase) compared to CIT alone ($p < 0.05$).

Concerning the inflammatory behaviour (Fig. 6), all gels did not induce pro-inflammatory effects at the level of the reconstituted nasal epithelium *in vitro*. In particular, PF-127/Carb-5-HA and PF-127/Carb-25-HA maintained TNF-α (Fig. 6A) and IL-1β (Fig. 6B) levels (expressed in pg/mL) close to the control values. In addition, PF-127/Carb-25-HA CIT and PF-127/Carb-5-HA CIT did not result in a significant increase in inflammatory markers compared to the control ($p < 0.05$), indicating the absence of a combination-induced inflammatory effect. PF-127/Carb-25-HA CIT has been shown to favourably modulate the inflammatory effect potentially associated with the administration of CIT, with a significant reduction in pro-inflammatory cytokine levels significantly compared to CIT alone (37% reduction; $p < 0.05$) and PF-127/Carb-5-HA (90% reduction; $p < 0.05$).

3.7. *Analysis of the biological effects of CIT gels on NBA in vitro model*

As reported in Fig. 6A, data obtained after 24h on an NBA *in vitro* model, based on the Transwell® co-culture of pNECs and SH-SY5Y neuronal lines, highlighted that both PF-127/Carb-5-HA and PF-127/Carb-25-HA did not compromise neuronal cell viability, but also showed a protective and stimulating effect compared to the control ($p < 0.05$). PF-127/Carb-5-HA CIT and PF-127/Carb-25-HA CIT maintained a favourable safety profile, highlighting a significant increase in the viability of SH-SY5Y cells compared to both the control and the respective vehicles ($p < 0.05$). Furthermore, PF-127/Carb-25-HA CIT showed statistically significant and superior data compared to free CIT

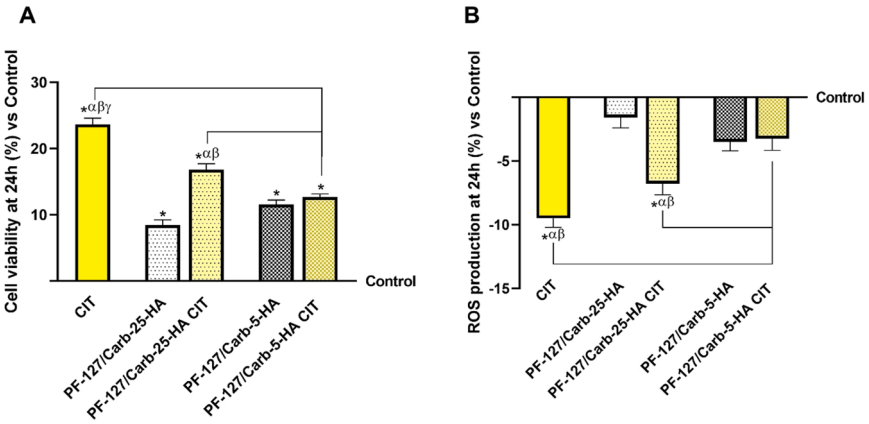


Fig. 4. Analysis of the biological effects of test samples in terms of cytotoxicity and oxidative stress after treatment for 24 h on pNEC epithelium. Cell viability results according to MTT assay (A); ROS production assessed by colorimetric method (B). Data are expressed as means ± SD (%) of increased values derived from five independent experiments performed in triplicate, normalised to control values (0% line). *$p < 0.05$ *vs* control; α $p < 0.05$ *vs* PF-127/Carb-25-HA; β $p < 0.05$ *vs* PF-127/Carb-5-HA; γ $p < 0.05$ *vs* P F-127/Carb-25-HA CIT; the bar $p < 0.05$ *vs* PF-127/Carb-5-HA.

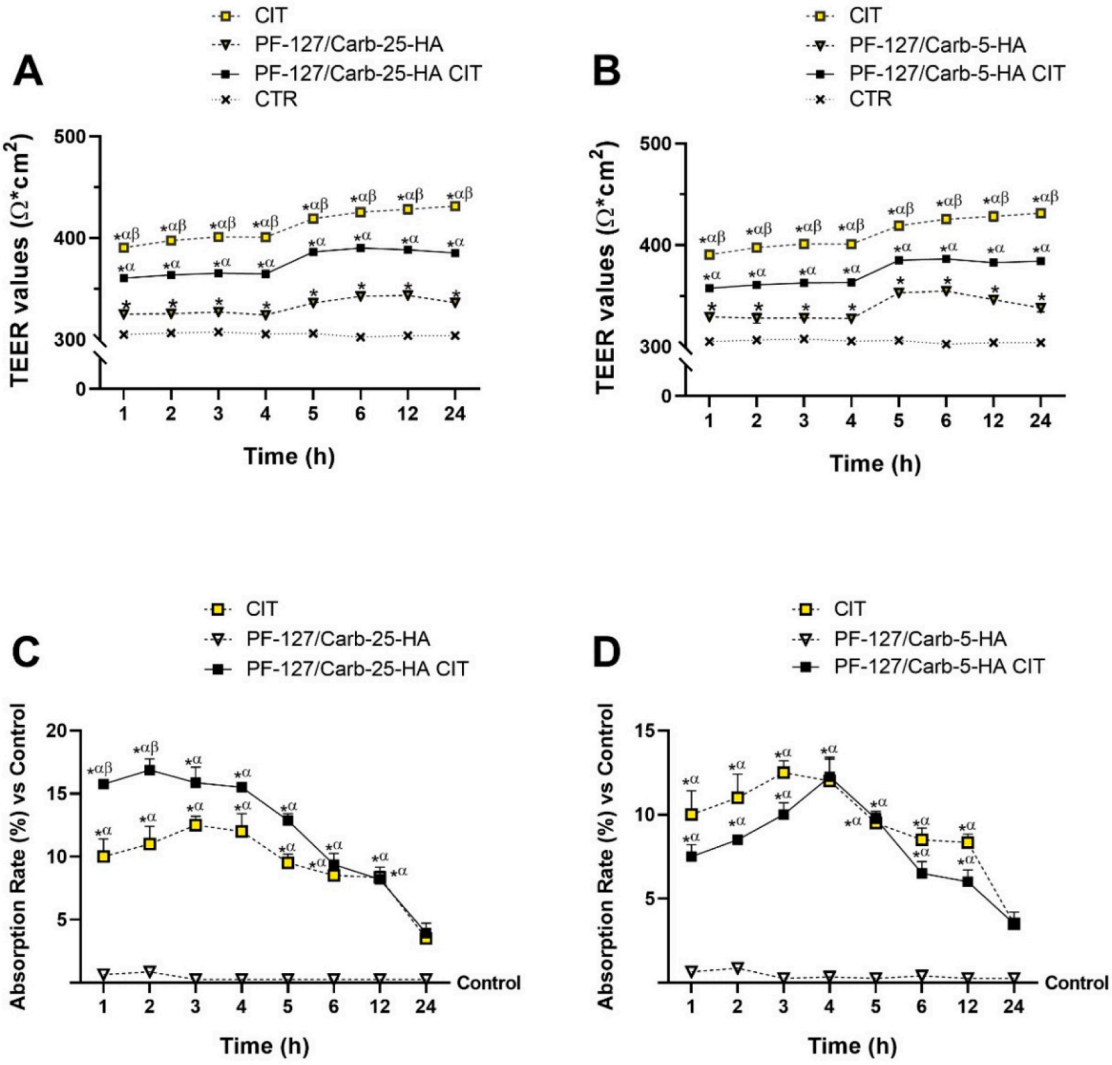


Fig. 5. Analysis of the biological effects of test samples on nasal epithelium integrity and permeability (absorption rate) after treatment for 24 h on pNECs epithelium. TEER analysis with EVOM3 instrument (A, B); permeability results arising from fluorescein sodium salt transport (C, D). Data are expressed as means ± SD (%) of increased values derived from five independent experiments performed in triplicate, normalised to control values. Only for (C, D), line 0% refers to the control. In (A, B) * $p < 0.05$ *vs* control; α $p < 0.05$ *vs* PF-127/Carb-25-HA; β $p < 0.05$ *vs* PF-127/Carb-25-HA CIT. In (C) * $p < 0.05$ *vs* control; α $p < 0.05$ *vs* PF-127/Carb-25-HA; β $p < 0.05$ *vs* free CIT. In (**D**) * $p < 0.05$ *vs* control; α $p < 0.05$ *vs* PF-127/Carb-5-HA.

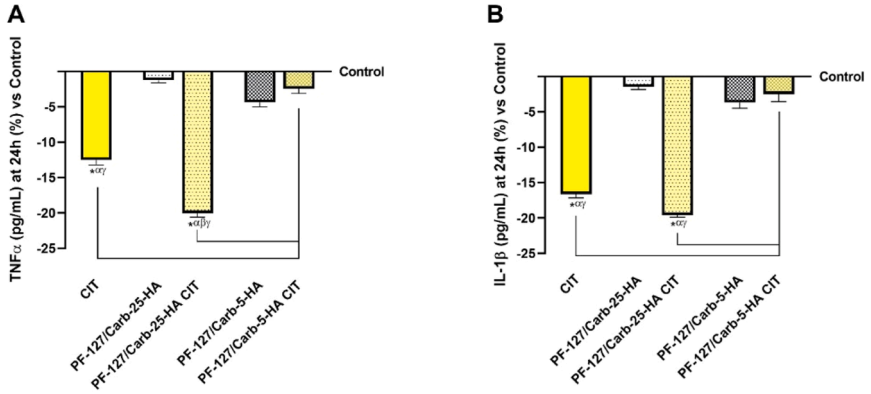


Fig. 6. Analysis of the biological effects of test samples on inflammatory response after treatment for 24h on pNECs epithelium. TNF-α levels (A) and IL-1β levels (B), both obtained via ELISA kit. Data are expressed as means ± SD (%) of increased values derived from five independent experiments performed in triplicate, normalised to control values (0% line). * $p < 0.05$ *vs* control; α $p < 0.05$ *vs* PF-127/Carb-25-HA; β $p < 0.05$ *vs* free CIT; γ $p < 0.05$ *vs* PF-127/Carb-5-HA; the bar $p < 0.05$ *vs* PF-127/Carb-25-HA CIT.

(20% increase; p < 0.05) and PF-127/Carb-5-HA (36.7% increase; $p < 0.05$).

In addition, regarding the intracellular levels of SOD1, all the samples examined showed an effective ability to limit enzyme levels, keeping them below 10% compared to the control, especially CIT-loaded gels (Fig. 7C) which showed significantly higher efficacy than the corresponding unloaded gels ($p < 0.05$) with data comparable to CIT alone.

Subsequently, modulations of the inflammatory state were conducted at the neuronal level in the NBA model (Fig. 8). All the samples analysed did not highlight any pro-inflammatory effect, confirming their safety in terms of cellular inflammatory response on TNF-α and IL-1β levels. In particular, PF-127/Carb-5-HA CIT and PF-127/Carb-25-HA CIT resulted in a significant reduction in neuronal inflammatory markers compared to the control ($p < 0.05$), indicating a potentially neuroprotective and anti-inflammatory effect. PF-127/Carb-25-HA CIT showed statistically significant and superior data compared to free CIT alone (51% reduction; $p < 0.05$) and PF-127/Carb-5-HA CIT (43% reduction; $p < 0.05$).

Finally, the study examined after 24 hours of treatment of the same experimental conditions the biological effects on the SIRT1 marker associated with the protection of neurons from damage and degeneration (Zhang et al., 2014). All samples examined evidenced the ability to positively modulate intracellular levels of SIRT1 (Fig. 9). Unloaded gels maintained SIRT1 levels comparable to those of the control, suggesting a good biocompatibility profile and absence of negative effects on the regulation of this protein. More significantly, PF-127/Carb-5-HA CIT and PF-127/Carb-25-HA CIT resulted in a statistically relevant increase in SIRT1 expression compared to control and gel vehicles ($p < 0.05$), indicating potential synergism between polymer vehicles and the active ingredient, CIT. Among the combinations tested, the PF-127/Carb-25-HA CIT showed the greatest effectiveness in enhancing the effect of CIT alone on the modulation of SIRT1 levels, with significant differences compared to treatment with CIT (25% increase; $p < 0.05$) and PF-127/Carb-5-HA CIT (46% increase; $p < 0.05$).

4. Discussion

In the present work, gel-forming systems for the intranasal administration of the antioxidant CIT were designed, prepared, and characterized with the aim of developing a pharmaceutical dosage form capable of enhancing the absorption of this antioxidant through the "nose-to-brain" delivery pathway. In formulating the gels, Carb was tested at concentrations of 5 and 25 mg/mL (corresponding to 3.9% and 17.1% w/w for PF-127/Carb-5-HA CIT and PF-127/Carb-25-HA CIT,

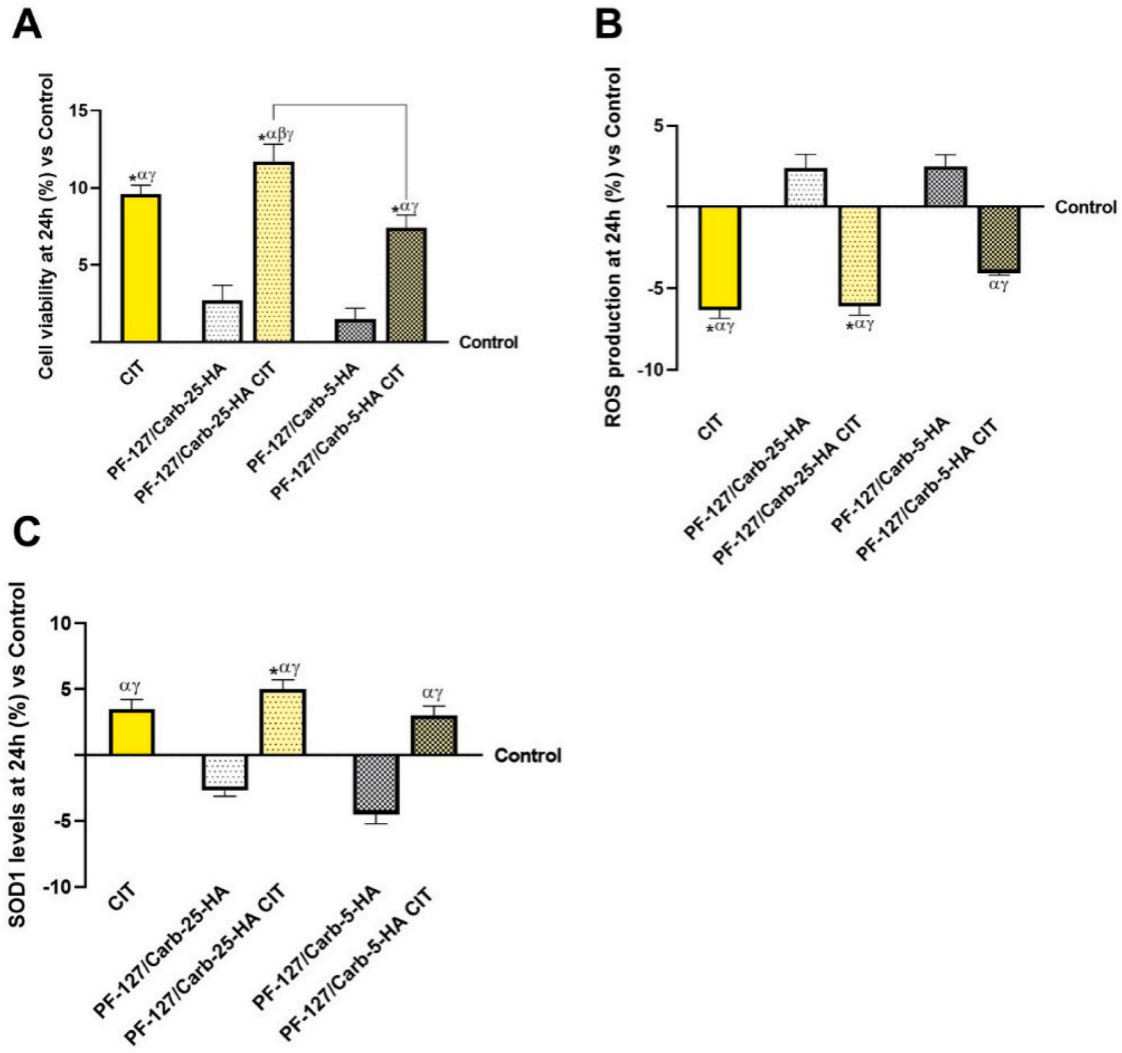


Fig. 7. Analysis of the biological effects of test samples on neuronal cell viability and oxidative stress after treatment for 24h in NBA *in vitro* model. Cell viability results through MTT assay (A); ROS production by colorimetric method (B); SOD1 levels results obtained through ELISA kit (C). Data are expressed as means ± SD (%) of increased values derived from five independent experiments performed in triplicate, normalised to control values (0% line). * $p < 0.05$ *vs* control; α $p < 0.05$ *vs* PF-127/Carb-25-HA; β $p < 0.05$ *vs* free CIT; γ $p < 0.05$ *vs* PF-127/Carb-5-HA; the bar $p < 0.05$ *vs* PF-127/Carb-5-HA CIT.

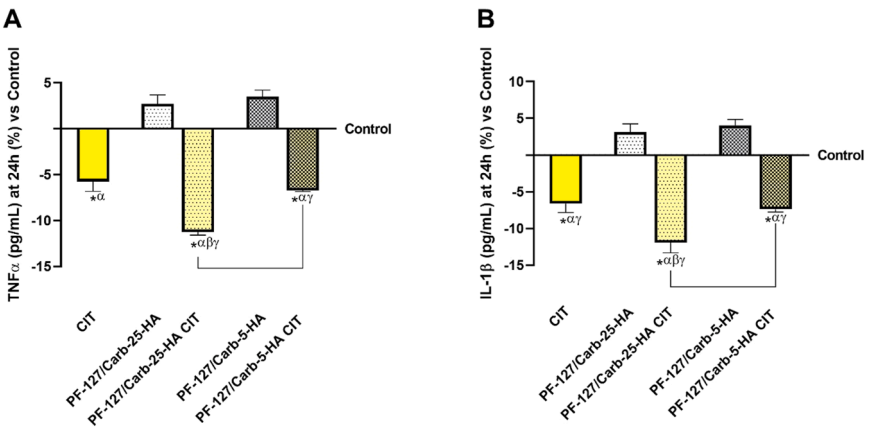


Fig. 8. Analysis of the biological effects of test samples on neuroinflammatory response after treatment for 24h on an *in vitro* model of nose-brain axis. TNF-α levels (A) and in IL-1β levels (B), both obtained via ELISA kit. Data are expressed as means ± SD (%) of increased values derived from five independent experiments performed in triplicate, normalised to control values (0% line). * $p < 0.05$ *vs* control; α $p < 0.05$ *vs* PF-127/Carb-25-HA; β $p < 0.05$ *vs* free CIT; γ $p < 0.05$ *vs* PF-127/Carb-5-HA; the bar $p < 0.05$ *vs* PF-127/Carb-5-HA CIT.

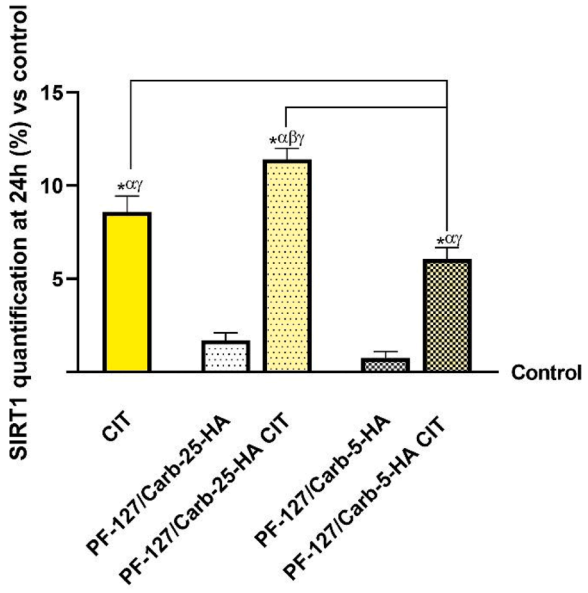


Fig. 9. Analysis of the biological effects of gels on neuroprotection (SIRT1 levels via ELISA kit) after treatment for 24h on an *in vitro* model of NBA. Data are expressed as means ± SD (%) of increased values derived from five independent experiments performed in triplicate, normalised to control values (0% line). * $p < 0.05$ *vs* control; α $p < 0.05$ *vs* PF-127/Carb-25-HA; β $p < 0.05$ *vs* free CIT; γ $p < 0.05$ *vs* PF-127/Carb-5-HA; the bar $p < 0.05$ *vs* PF-127/Carb-5-HA CIT.

respectively), while PF-127 was kept constant at 110 mg/mL (corresponding to 87.3% and 75.3% w/w for PF-127/Carb-5-HA CIT and PF-127/Carb-25-HA CIT, respectively).

From the osmolarity measurement viewpoint, no issue arose for the PF-127/Carb-5-HA CIT gel, whereas the higher viscosity associated with the PF-127/Carb-25-HA CIT gel limited us in performing the experimental determination of osmolarity value according to the protocol followed and, consequently, in predicting possible irritation connected to the osmotic stress.

Gels were also examined for their SEM morphology and, as shown in the microphotographs (Fig. 1A–D), it appeared that Carb polymer concentration primarily determines the network density and porosity, while the presence of CIT tends to enhance structural uniformity and surface smoothness. Hence, from SEM observations PF-127/Carb-25-HA CIT resulted in a consolidated and tightly packed structure (Fig. 1D), differently from PF-127/Carb-5-HA CIT that appeared as a loosely interconnected porous network (Fig. 1C).

Furthermore, to gain insights into the behavior of the pre-gelled systems, their mechanical characterization was also carried out and the properties of their components were also elucidated. It is well known that PF-127, a triblock copolymer, undergoes a well-known temperature-dependent sol–gel transition; namely, as its concentration increases, PF-127 solutions experience a two-step transformation: first from a solution to a micellar suspension, and then from a micellar suspension to a soft gel as micelles become densely packed at high volume fractions. Below its gelation temperature—*i.e.*, the temperature at which the sol–gel transition occurs—PF-127 behaves as a Newtonian fluid with a constant viscosity across shear rates, as reported by Jalaal et al. (Jalaal et al., 2017).

Carb, on the other hand, undergoes a pH-dependent sol–gel transition. Upon neutralization (typically around pH 6–7), Carb particles swell and form a jammed network of microgels, giving rise to a gel-like structure (Di Giuseppe et al., 2015; Kim et al., 2003).

For both formulations PF-127/Carb-5-HA and PF-127/Carb-5-HA CIT, the sol–gel transition occurs at pH = 6 and T = 37°C, reflecting the physiological conditions of the nasal cavity. Under these conditions, the PF-127/Carb-5-HA CIT formulation forms a slightly less extensive gel structure.

Moreover, we found that the shear-viscosity curve of a further pre-gelled formulation prepared for needing connected to the mechanical studies and employing PF-127 at 11% w/w, Carb at 1% w/w, HA at 0.1% w/w and CIT at 1% w/w at T = 20°C and pH = 3.9 showed a pronounced decrease in viscosity with increasing shear rate, hence confirming that the material behaves as a structured viscous liquid (Fig. 2A). Such behavior is entirely consistent with the formulation conditions. Indeed, at the acidic pH of the system (pH 3.9), Carb is only weakly ionized and, therefore, exhibits minimal swelling, preventing the development of a percolated microgel network with significant elasticity (Di Giuseppe et al., 2015; Jaworski et al., 2022). At the same time, the concentration of PF-127 herein used (11% w/w) is below the threshold required to induce thermo-gelation at 20 °C (Fakhari et al., 2017); even if micellization is already partially established at this temperature, the micelles remain unjammed and do not give rise to a gel (Jones et al., 2009) present only at 0.1% w/w, is far too dilute to produce any appreciable rheological effect (Mayol et al., 2008). Altogether, the observed response reflects the essentially additive behavior of the individual components, with no detectable synergistic thickening or emergent structuring beyond what each polymer contributes independently.

The liquid-like behavior of the PF127/Carb-1-HA CIT formulation at

20°C seemed particularly advantageous for intranasal delivery. Under storage conditions, the system remained sufficiently fluid to be easily pumped and atomized, ensuring smooth spraying and effective deposition within the nasal cavity. Once administered, however, the formulation could encounter the physiological environment (approximately 37°C and a pH close to 7 (England et al., 1999) which triggers its transition from a viscous liquid to a gel-like material. This sol-to-gel transformation is a key functional feature of the system: it greatly facilitates administration while subsequently enhancing residence time on the nasal mucosa, thereby improving the in-situ retention and release profile of CIT.

As for the PF-127/Carb-5-HA CIT gel, it was seen that for these CIT-containing systems a pH- and temperature-triggered sol–gel transition occurred, forming a weak physical gel in the case of PF-127/Carb-5-HA CIT resembling the PF127/Carb-1-HA CIT formulation with enhanced viscous behavior. while a stronger physical gel formed in the case of PF-127/Carb-25-HA CIT due to the higher Carb concentration utilized. This behavior is consistent with known effects in soft glassy materials, where additives such as drugs or amphiphilic molecules can act as spacers or lubricants, disrupting the gel network and enhancing viscous contributions. The unchanged G″ shown in Fig. 2B implies that frictional losses remain stable, while the reduced G′ reflects a less interconnected elastic structure. However, a limitation of the mechanical investigations herein reported is related to the fact that Carb solubilization in aqueous medium at concentrations higher than 1% w/w is difficult, and, hence, the rheological evaluation could not be performed in the case of both gel systems PF-127/Carb-25-HA and PF-127/Carb-25-HA CIT. Hence, from the rheological profile viewpoint, PF-127/Carb-5-HA CIT gel is particularly suited for nasal drug delivery, offering spread ability, softness, and controlled flow, while maintaining sufficient structure for mucosal retention and can be useful to achieve a localized release of CIT.

At this regard, to assess CIT delivery capability from the prepared gels, *in vitro* release tests (Fig. 3A) and permeation studies (Fig. 3B, Table 1) were performed. By mimicking the nasal compartment via the use of SNF as receiving medium, the *in vitro* release test evidenced the almost quantitative delivery of CIT within 48 h even though the CIT release from PF-127/Carb-25-HA CIT gel resulted slightly faster than that of PF-127/Carb-5-HA CIT (Fig. 3A). We believed that such outcome can be rationalized taking into account SEM analysis results suggesting that PF-127/Carb-25-HA CIT (Fig. 1D) displayed a highly compact and continuous surface, largely devoid of visible fissures or macroporous features unlike PF-127/Carb-5-HA CIT (Fig. 1C). Just due to the more compact structure of the former gel (Fig. 1D), it is possible that CIT is localized on the surface of the gel and, therefore, it is more prone to be released in the presence of release medium (SNF), while the presence of voids and less compact structure in PF-127/Carb-5-HA CIT (Fig. 1C) allows a deeper CIT localization in this last gel and, consequently, its slower release.

On the other hand, once the nasal porcine mucosa was employed for permeation studies (Fig. 3B, Table 1), the CIT amount delivered appeared significantly reduced. Indeed, *P*app values of CIT were in the range 7.2×10^{-3}–12.3×10^{-3} cm/sec and, as shown in Table 1, no statistical difference was noticed between the *P*app of free CIT and each one of the tested gels. On one side, the compact architecture and tight packing of the Carb matrix of the gels evidenced by SEM images (Fig. 1B and D), and on the other hand CIT hydrophilicity, can also justify the high percentages of CIT retained on the apical side. Hence, a low permeation of CIT across the nasal porcine mucosa was obtained (*i.e.*, in the range 7.8–9.5% of the initial CIT content), irrespective of the gel examined (Table 1). Furthermore, from Fig. 3B the low CIT permeation extent can also be deduced because the highest CIT flux obtained, in the case of PF-127/Carb-5-HA CIT, reached 0.15 mg substance/cm^2 after 24 hours. Although a limitation of this study can be represented by low CIT permeation (Fig. 3B), to the best of our knowledge, no *P*app of CIT referred to the nasal route has been previously reported in the literature. On the other hand, once delivered even if in low extent, CIT itself can restore the barrier function of endothelial cells compromised by hypoxia/aglycemia conditions, probably via up-regulating the expression of tight junction proteins in endothelial cells (Ma et al., 2013). As told, our work plan was based on the fact that we first aimed at verifying *ex vivo* CIT permeation across the nasal porcine mucosa and, as a following step, human cell model lines were adopted to obtain more reliable information on the biological effects elicited by CIT-containing gels.

From Fig. 4A, PF-127/Carb-25-HA CIT was seen to determine a relevant improvement in human nasal pNECs cell viability, with significantly higher values than both the control, the respective vehicle and PF-127/Carb-5-HA CIT ($p < 0.05$), suggesting that the association CIT–gel may represent a safe formulation at the nasal level.

Moreover, taking into account the permeability studies carried out in pNECs monolayer, it resulted that PF-127/Carb-25-HA CIT could predict an acceleration of the rate of absorption of CIT. On the other hand, PF-127/Carb-5-HA CIT (Fig. 6D) did not show any significant improvement in the absorption kinetics compared to free CIT, maintaining lower or overlapping absorption levels (only in the range 4 h–5 h and 24 h) with free CIT. Importantly, when MTT test was carried out in an *in vitro* NBA model (Fig. 7A), the results evidenced a potential synergistic effect between the carrier gel and CIT, capable of improving the effectiveness of CIT at the neuronal level, after its crossing of the nasal epithelium. Furthermore, Fig. 7B indicates that ROS production in the SH-SY5Y cell line was kept below 5%, with better data comparable to CIT alone for PF-127/Carb-25-HA CIT and slightly lower values for PF-127/Carb-5-HA CIT. Relevantly, the results of the modulation of the inflammatory state (Fig. 9) suggest that both CIT-containing gels can effectively modulate the neuronal inflammatory response, thus representing a promising approach for the protection of nerve cells in pathological contexts characterized by inflammation, as occurs in PD. Although the limitations above mentioned, overall, the results obtained outline a biological influence at the neuronal level given by the components of the gels, which have proven to maintain the integrity of the nasal epithelium (Fig. 5). Indeed, the tested gel formulations contain PF-127 and Carb, which can contribute to interaction with the cell membrane and increase viscosity and structural stability, respectively, at the epithelial interface. Strictly connected to this process, SIRTI1 level evaluation (Fig. 9), determined after transepithelial transport of the formulations through the nasal epithelium, provided further insights into the neurobiological effects of the gel formulations. In other words, in the gel the presence of PF-127 which improves membrane permeability and Carb which provides high viscosity (Aggarwal and Nagpal, 2018) also elicit important effects in the SH-SY5Y cells and, hence, the gel systems may facilitate the release and activity of CIT along the nose-brain pathway. As known, the co-culture pNECs/SH-SY5Y is not a model of BBB instead of Human Brain Microvascular Endothelial Cells (HBMECs), where a selective physiological interface regulates the substances passage between the bloodstream and the CNS (Guaragnella et al. 2026; Wang et al., 2020; Eigenmann et al., 2016). In this context, the present study discloses new research perspectives addressed to explore CIT permeability across the BBB, once the antioxidant is released from the examined gels.

5. Conclusions

In the present work, two new gel formulations consisting of PF-127/Carb-5-HA CIT and PF-127/Carb-25-HA CIT were prepared and *in vitro* characterized from a physicochemical and biological point of view. In detail, from our study the behavior of such gels proved to be particularly suitable for nasal drug delivery and useful to achieve a localized release of CIT. Both gels *i)* possess pH values close to those recognized as safe for that mucosa; *ii)* were able to release the antioxidant CIT in quantitative amount after 48 h in SNF. Moreover, the gel biological effects were screened in two cell model lines, namely pNECs and SH-SY5Y cell lines, because this integrated approach allowed us to assess the biocompatibility of the nasal application of CIT formulations and explore their potential neuronal effects. Definitely, the formulation PF-127/Carb-25-

HA CIT resulted *in vitro* in the most promising formulation for CIT administration by intranasal route, and its main benefit could be envisaged in the opportunity to provide self-medication for patients. Nevertheless, even the profile of the PF-127/Carb-5-HA CIT formulation is ~~also~~ of interest, although the biological performance of this gel resulted slightly lower than that of the PF-127/Carb-25-HA CIT one. Indeed, it should also be taken into account that PF-127/Carb-5-HA CIT formulation could possess the distinctive advantage of allowing the use of devices able to target the upper nasal region such as Vianase™ Optinose™ and Precision Olfactory Delivery (POD®) technology due to its rheological features of weak physical gel/viscous liquid-like state, thus promoting the "nose-to-brain delivery" transport pathway.

CRediT authorship contribution statement

Anna Patrizia de Nichilo: Investigation. **Francesca Uberti:** Writing – review & editing, Writing – original draft, Supervision, Methodology, Conceptualization. **Adriana Trapani:** Writing – review & editing, Writing – original draft, Supervision, Investigation, Funding acquisition, Conceptualization. **Stefano Castellani:** Writing – review & editing, Formal analysis. **Giorgia Iaconisi:** Methodology, Investigation, Formal analysis. **Giorgia Franzino:** Methodology, Investigation. **Cinzia Di Franco:** Software, Investigation. **Lorenzo Guerra:** Investigation. **Rosanna Mallamaci:** Writing – review & editing. **Rosa Angela Cardone:** Methodology, Investigation. **Carmelo Ventra:** Resources. **Domenico Larobina:** Validation, Investigation. **Loredana Capobianco:** Validation, Investigation. **Simone Mulè:** Methodology. **Elvira De Giglio:** Methodology, Investigation.

Declaration of competing interest

The authors declare the following financial interests/personal relationships which may be considered as potential competing interests:

Adriana Trapani reports equipment, drugs, or supplies was provided by University of Bari Department of Pharmacy and Pharmacology. Adriana Trapani reports a relationship with University of Bari Department of Pharmacy and Pharmacology that includes: employment. If there are other authors, they declare that they have no known competing financial interests or personal relationships that could have appeared to influence the work reported in this paper.

Acknowledgements

A.T. would like to acknowledge Dr. Fabio Feolo and Dr. Massimo Mastropasqua (University of Bari-Aldo Moro, Bari, Italy) for their technical skills. The authors would also acknowledge Dr. Daniele Bernareggi and Dr. Marco Isgro' (IMCD, SpA, Milan, Italy) for Carbopol gift.

Data availability

The authors declare they have no known competing financial interests or personal relationships that could have appeared to influence the work reported in this paper.

References

Abou Elhassan, K.M., Sarhan, H.A., Hussein, A.K., Taye, A., Ahmed, Y.M., Safwat, M.A., 2022. Brain targeting of citicoline sodium via hyaluronic acid-decorated novel nano-transbilosomes for mitigation of Alzheimer's disease in a rat model: formulation, optimization, *in vitro* and *in vivo* assessment. Int. J. Nanomed. 17, 6347–6376.

Aggarwal, G., Nagpal, M., 2018. Pharmaceutical polymer gels in drug delivery. In: Thakur, V.K., Thakur, M.K., Voicu, S.I. (Eds.), Polymer Gels: Perspectives and Applications. Springer Singapore, Singapore, pp. 249–284.

Barron, S.L., Saez, J., Owens, R.M., 2021. *vitro* Models for Studying Respiratory Host-Pathogen Interactions. Adv. Biol. (Weinh) 5, e2000624.

Bekhet, M.A., Ali, A.A., Kharshoum, R.M., El-Ela, F.I.A., Salem, H.F., 2022. Intranasal niosomal in situ gel as a novel strategy for improving citicoline efficacy and brain delivery in treatment of epilepsy: *in vitro* and *ex vivo* characterization and *in vivo* pharmacodynamics investigation. J. Pharm. Sci. 111, 2258–2269.

Cassano, R., Trapani, A., Di Gioia, M.L., Mandracchia, D., Pellitteri, R., Tripodo, G., Trombino, S., Di Gioia, S., Conese, M., 2020. Synthesis and characterization of novel chitosan-dopamine or chitosan-tyrosine conjugates for potential nose-to-brain delivery. Int. J. Pharm. 589, 119829.

Castellani, S., Iaconisi, G.N., Tripaldi, F., Porcelli, V., Trapani, A., Messina, E., Guerra, L., Di Franco, C., Maruccio, G., Monteduro, A.G., Corbo, F., Di Gioia, S., Trapani, G., Conese, M., 2024a. Dopamine and citicoline-co-loaded solid lipid nanoparticles as multifunctional nanomedicines for parkinson's disease treatment by intranasal administration. Pharmaceutics 16, 1048.

Castellani, S., Mallamaci, R., De Giglio, E., Caponio, A., Guerra, L., Fracchiolla, G., Trapani, G., Kristan, K., Cardone, R.A., Passantino, G., Zizzo, N., Franzino, G., Larobina, D., Trapani, A., Conese, M., 2024b. Slightly viscous dispersions of mucoadhesive polymers as vehicles for nasal administration of dopamine and grape seed extract-loaded solid lipid nanoparticles. Int. J. Pharm. 659, 124255.

Crowe, T.P., Hsu, W.H., 2022. Evaluation of recent intranasal drug delivery systems to the central nervous system. Pharmaceutics. 14, 629.

Di Giuseppe, E., Corbi, F., Funiciello, F., Massmeyer, A., Santimano, T.N., Rosenau, M., Davaille, A., 2015. Characterization of Carbopol® hydrogel rheology for experimental tectonics and geodynamics. Tectonophysics 642, 29–45.

Dorsey, E.R., De Miranda, B.R., Horsager, J., Borghammer, P., 2024. The body, the brain, the environment, and Parkinson's disease. J. Parkinsons. Dis. 14, 363–381.

Eigenmann, D.E., Jahne, E.A., Smiesko, M., Hamburger, M., Oufir, M., 2016. Validation of an immortalized human (hBMEC) in vitro blood-brain barrier model. Anal. Bioanal. Chem. 408, 2095–2107.

England, R.J., Homer, J.J., Knight, L.C., Ell, S.R., 1999. Nasal pH measurement: a reliable and repeatable parameter. Clin. Otolaryngol. Allied. Sci. 24, 67–68.

Fakhari, A., Corcoran, M., Schwarz, A., 2017. Thermogelling properties of purified poloxamer. Heliyon 3 (3), e00390.

Ferrari, S., Mule, S., Galla, R., Brovero, A., Genovese, G., Molinari, C., Uberti, F., 2024. Effects of nutraceutical compositions containing Rhizoma gastrodiae or lipoic acid in an *in vitro* induced neuropathic pain model. Int. J. Mol. Sci. 25.

Galla, R., Ferrari, S., Miletto, I., Mule, S., Uberti, F., 2025. *In vitro* neuroprotective effects of a mixed extract of bilberry, Centella asiatica, Hericium erinaceus, and palmitoylethanolamide. Foods. 14.

Galla, R., Grisenti, P., Farghali, M., Saccuman, L., Ferraboschi, P., Uberti, F., 2021. Ovotransferrin supplementation improves the iron absorption: an *in vitro* gastro-intestinal model. Biomedicines 9, 1543.

Galla, R., Ruga, S., Aprile, S., Ferrari, S., Brovero, A., Grosa, G., Molinari, C., Uberti, F., 2022. New hyaluronic acid from plant origin to improve joint protection-an *in vitro* study. Int. J. Mol. Sci. 23.

Garcia-Lopez, C., Garcia-Lopez, V., Matamoros, J.A., Fernandez-Albarral, J.A., Salobrar-Garcia, E., de Hoz, R., Lopez-Cuenca, I., Sanchez-Puebla, L., Ramirez, J.M., Ramirez, A.I., Salazar, J.J., 2023. The Role of Citicoline and Coenzyme Q10 in Retinal. Pathology. Int. J. Mol. Sci. 24.

Guaragnella, N., Coppola, C., Fasano, D., Castellani, S., Mallamaci, R., Musaro', D., Greco, M., Primavera, A., Capobianco, L., Cioffi, N., Mesto, E., Schingaro, E., Colangelo, G., Trapani, A., Maffia, M., 2026. Nanostructured lipid carriers containing Dopamine and Grape Seed Extract: evaluation of cell line-based models with application to Parkinson disease studies. J. Drug Deliv. Sci. Technol. 120, 108187.

Hamdy, S.M., Elsayed, N.A., Youness, E.R., Elesh, H.M.R., Abdel-Salam, O.M.E., 2025. Effect of cytidine-5′-diphosphocholine alone, caffeine or their combination on oxidative stress and inflammatory response in an experimentally-induced Parkinson's disease. J. Complement. Integr. Med. 22, 479–489.

Hinz, F.I., Villegas, C.L.M., Roberts, J.T., Yao, H., Gaddam, S., Delwig, A., Green, S.A., Fredrickson, C., Adrian, M., Asuncion, R.R., Cheung, T.K., Hayne, M., Hackos, D.H., Rose, C.M., Richmond, D., Hoogenraad, C.C., 2024. Context-specific stress causes compartmentalized SARM1 activation and local degeneration in cortical neurons. J. Neurosci. 44, e2424232024. Italian patent N.102025000010455, r.o.

Jalaal, M., Cottrell, G., Balmforth, N., Stoeber, B., 2017. On the rheology of Pluronic F127 aqueous solutions. J. Rheol. (N. Y. N. Y) 61, 139–146.

Jaworski, Z., Spychaj, T., Story, A., Story, G., 2022. Carbomer microgels as model yield-stress fluids 38, 881–919.

Jones, D.S., Bruschi, M.L., de Freitas, O., Gremiao, M.P., Lara, E.H., Andrews, G.P., 2009. Rheological, mechanical and mucoadhesive properties of thermoresponsive, bioadhesive binary mixtures composed of poloxamer 407 and carbopol 974P designed as platforms for implantable drug delivery systems for use in the oral cavity. Int. J. Pharm. 372, 49–58.

Khan, T.U., Mushtaq, N., Iqbal, T., Liu, C.G., 2026. Mucoadhesive hyaluronic acid composites for prolonged gastric retention. Int. J. Pharm. 687, 126371.

Kim, J.Y., Song, J.Y., Lee, E.J., Park, S.K., 2003. Rheological properties and microstructures of Carbopol gel network system. Colloid. Polym. Sci. 281, 614–623.

King, J., Giselbrecht, S., Truckenmuller, R., Carlier, A., 2021. Mechanistic computational models of epithelial cell transporters-the adorned heroes of pharmacokinetics. Front. Pharmacol. 12, 780620.

Koo, J., Lim, C., Oh, K.T., 2024. Recent advances in intranasal administration for brain-targeting delivery: a comprehensive review of lipid-based nanoparticles and stimuli-responsive gel formulations. Int. J. Nanomed. Volume 19, 1767–1807.

Kovalevich, J., Langford, D., 2013. Considerations for the use of SH-SY5Y neuroblastoma cells in neurobiology. Methods Mol. Biol. 1078, 9–21.

Lazarini, F., Roze, E., Lannuzel, A., Lledo, P.M., 2022. The microbiome-nose-brain axis in health and disease. Trends Neurosci. 45, 718–721.

Ma, X., Zhang, H., Pan, Q., Zhao, Y., Chen, J., Zhao, B., Chen, Y., 2013. Hypoxia/Aglycemia-induced endothelial barrier dysfunction and tight junction protein downregulation can be ameliorated by citicoline. PLoS One 8, e82604.

Margari, A., Monteduro, A.G., Rizzato, S., Capobianco, L., Crestini, A., Rivabene, R., Piscopo, P., D'Onofrio, M., Manzini, V., Trapani, G., Quarta, A., Maruccio, G., Ventra, C., Lieto, L., Trapani, A., 2022. The encapsulation of citicoline within solid lipid nanoparticles enhances its capability to counteract the 6-hydroxydopamine-induced cytotoxicity in human neuroblastoma SH-SY5Y cells. Pharmaceutics 14.

Martens, A., Amann, G., Schmidt, K., Gaupmann, R., Bohm, B., Dehlink, E., Szepfalusi, Z., Forster-Waldl, E., Berger, A., Fyhrquist, N., Alenius, H., Wisgrill, L., 2019. An optimized, robust and reproducible protocol to generate well-differentiated primary nasal epithelial models from extremely premature infants. Sci. Rep. 9, 20069.

Mayol, L., Quaglia, F., Borzacchiello, A., Ambrosio, L., La Rotonda, M.I., 2008. A novel poloxamers/hyaluronic acid in situ forming hydrogel for drug delivery: rheological, mucoadhesive and *in vitro* release properties. Eur. J. Pharm. Biopharm. 70, 199–206.

Molinari, C., Ruga, S., Farghali, M., Galla, R., Bassiouny, A., Uberti, F., 2021. Preventing c2c12 muscular cells damage combining magnesium and potassium with vitamin D3 and curcumin. J. Tradit. Complement. Med. 11, 532–544.

Moratin, H., Lang, J., Picker, M.S., Rossi, A., Wilhelm, C., von Fournier, A., Stoth, M., Goncalves, M., Kleinsasser, N., Hackenberg, S., Scherzad, A., Meyer, T.J., 2025. The impact of NO(2) on epithelial barrier integrity of a primary cell-based air-liquid interface model of the nasal respiratory epithelium. J. Appl. Toxicol. 45, 482–491.

Mou, Y.K., Song, X.Y., Wang, H.R., Wang, Y., Liu, W.C., Yang, T., Zhang, M.J., Hu, Y., Ren, C., Song, X.C., 2024. Understanding the nose-brain axis and its role in related diseases: a conceptual review. Neurobiol. Dis. 202, 106690.

Mura, P., Mennini, N., Nativi, C., Richichi, B., 2018. In situ mucoadhesive-thermosensitive liposomal gel as a novel vehicle for nasal extended delivery of opiorphin. Eur. J. Pharm. Biopharm. 122, 54–61.

Nantachit, N., Sunintaboon, P., Ubol, S., 2016. Responses of primary human nasal epithelial cells to EDIII-DENV stimulation: the first step to intranasal dengue vaccination. Virol. J. 13, 142.

Parisi, V., Oddone, F., Ziccardi, L., Roberti, G., Coppola, G., Manni, G., 2018. Citicoline and retinal ganglion cells: effects on morphology and function. Curr. Neuropharmacol. 16, 919–932.

Pichla, M., Pulaski, L., Kania, K.D., Stefaniuk, I., Cieniek, B., Pienkowska, N., Bartosz, G., Sadowska-Bartosz, I., 2020. Nitroxide radical-containing redox nanoparticles protect neuroblastoma SH-SY5Y cells against 6-hydroxydopamine toxicity. Oxid. Medicine Cellular Longevity 2020, 9260748.

Que, D.S., Jamora, R.D.G., 2021. Citicoline as adjuvant therapy in Parkinson's disease: a systematic review. Clin. Ther. 43, e19–e31.

Roberti, G., Tanga, L., Parisi, V., Sampalmieri, M., Centofanti, M., Manni, G., 2014. A preliminary study of the neuroprotective role of citicoline eye drops in glaucomatous optic neuropathy. Indian J. Ophthalmol. 62, 549.

Salmina, A.B., Kharitonova, E.V., Gorina, Y.V., Teplyashina, E.A., Malinovskaya, N.A., Khilazheva, E.D., Mosyagina, A.I., Morgun, A.V., Shuvaev, A.N., Salmin, V.V., Lopatina, O.L., Komleva, Y.K., 2021. Blood-brain barrier and neurovascular unit *in vitro* models for studying mitochondria-driven molecular mechanisms of neurodegeneration. Int. J. Mol. Sci. 22, 4661.

Sathyamurthy, V.H., Nagarajan, Y., Parvathi, V.D., 2024. Mitochondria-endoplasmic reticulum contact sites (MERCS): a new axis in neuronal degeneration and regeneration. Mol. Neurobiol. 61, 6528–6538.

Singh, B., Kumar, A., Rohit, 2020. Synthesis and characterization of alginate and sterculia gum based hydrogel for brain drug delivery applications. Int. J. Biol. Macromol. 148, 248–257.

Srividya, B., Cardoza, R.M., Amin, P.D., 2001. Sustained ophthalmic delivery of ofloxacin from a pH triggered in situ gelling system. J. Control Release 73, 205–211.

Teixeira, J., Lumack do Monte, Z., Tenreiro, S., Salema-Oom, M., Silva, D.C., Saramago, B., Paula Serro, A., 2024. Citicoline eluting hydrogels for therapeutic contact lenses intended to treat neurodegenerative diabetic ocular diseases. Int. J. Pharm. 667, 124908.

Trapani, A., Castellani, S., Guerra, L., De Giglio, E., Fracchiolla, G., Corbo, F., Cioffi, N., Passantino, G., Poeta, M.L., Montemurro, P., Mallamaci, R., Cardone, R.A., Conese, M., 2023. Combined dopamine and grape seed extract-loaded solid lipid nanoparticles: nasal mucosa permeation, and uptake by olfactory ensheathing cells and neuronal SH-SY5Y Cells. Pharmaceutics. 15, 881.

Uberti, F., Trotta, F., Pagliaro, P., Bisericaru, D.M., Cavalli, R., Ferrari, S., Penna, C., Matencio, A., 2023. Developing new cyclodextrin-based nanosponges complexes to improve vitamin D absorption in an *in vitro* Study. Int. J. Mol. Sci. 24, 5322.

van Brummelen, R., van Brummelen, A.C., 2025. The role of neuro-supportive substances of natural origin in neurological conditions-A literature-based formulators' perspective. Front. Neurol. 16, 1647092.

Wang, G., Wang, J., Guan, R., 2020. Novel phospholipid-based labrasol nanomicelles loaded flavonoids for oral delivery with enhanced penetration and anti-brain tumor efficiency. Curr. Drug Deliv. 17, 229–245.

Wu, H.C., Hu, Q.L., Zhang, S.J., Wang, Y.M., Jin, Z.K., Lv, L.F., Zhang, S., Liu, Z.L., Wu, H.L., Cheng, O.M., 2018. Neuroprotective effects of genistein on SH-SY5Y cells overexpressing A53T mutant alpha-synuclein. Neural Regener. Res. 13, 1375–1383.

Xu, X., Zhang, A., Li, N., Li, P.L., Zhang, F., 2015. Concentration-dependent diversifcation effects of free cholesterol loading on macrophage viability and polarization. Cell Physiol. Biochem. 37, 419–431.

Zhang, J., Feng, X., Wu, J., Xu, H., Li, G., Zhu, D., Yue, Q., Liu, H., Zhang, Y., Sun, D., Wang, H., Sun, J., 2014. Neuroprotective effects of resveratrol on damages of mouse cortical neurons induced by beta-amyloid through activation of SIRT1/Akt1 pathway. BioFactors 40, 258–267.